Fabrication and characterization of deep mesa etched "anti"-dot superlattices in GaAs-AlGaAs heterostructures

D. Weiss,[a] P. Grambow, and K. von Klitzing
Max–Planck-Institut für Festkörperforschung, D-7000 Stuttgart 80, Germany

A. Menschig
IV Physikalisches Institut der Universität Stuttgart, D-7000 Stuttgart 80, Germany

G. Weimann
Walter–Schottky Institut der TU München, D-8046 Garching, Germany

(Received 8 February 1991; accepted for publication 29 March 1991)

By etching a periodic array of holes through a high-mobility two-dimensional electron gas we define a lateral, "anti"-dot-type superlattice with periods $a = 200$ and $a = 300$ nm, much smaller than the electron mean free path in the unpatterned material. The devices are fabricated using electron beam lithography and reactive ion etching techniques, and characterized by magnetotransport experiments. Commensurability effects and the observed quenching of the Hall effect indicate that the electron gas between the etched holes essentially maintains its initial high electron mobility.

Artificial lateral superlattices (LSLs), fabricated from high-mobility GaAs-AlGaAs heterojunctions, are of interest for studying, e.g., phenomena such as Bloch oscillations or, in the presence of a magnetic field, Hofstadter's[1] electron energy spectrum. From a more device-oriented point of view negative resistance devices[2] or the suppression of optical phonon scattering in suitably tailored LSL might be promising.[3] Such superlattices have been defined by holographic techniques,[4] electron beam lithography,[5,6] x-ray lithography,[7] direct focused ion beam writing,[8] or by using monolayers of periodically arranged organic molecules.[9] Another possibility might be the use of vicinial semiconductor surfaces to grow lateral superlattices with periods in the 10 nm range.[10] The realization of such laterally periodic nanostructures has been reviewed recently.[11]

In this letter we describe the fabrication of a LSL using a combination of electron beam lithography and dry etching techniques. The starting material for the LSL are conventional high-mobility GaAs-AlGaAs heterostructures with carrier densities N_s between 2.2×10^{11} cm^{-2} and 3×10^{11} cm^{-2}. The corresponding mobilities μ range from 0.56×10^{6} cm^2/V s to 1.2×10^{6} cm^2/V s measured in dark in an unpatterned Hall bar at liquid-helium temperatures. A typical sample "sandwich" consists of a 20 nm undoped GaAs cap layer, 30–50 nm Si-doped (typically $\sim5\times10^{18}$ cm^{-3}) AlGaAs (Al content $\sim$33%), 19–40 nm undoped AlGaAs spacer layer, and 1–4 μm GaAs grown on a semi-insulating substrate. In order to fabricate large LSL areas (200 μm$\times$500 μm) with uniform "anti"-dot shapes and constant superlattice period we have defined the pattern by electron beam lithography, sketched schematically in Fig. 1(a). After standard cleaning procedures the sample material is spin coated with 200 nm polymethylmethacrylate (PMMA) positive tone resist. With a JEOL JBX5DII(U) high-resolution electron beam vector scanner, we exposed single points within the area exposure mode (30 000–52 000 μC/cm^2, depending on the area filling factor) to define the dot pattern in the resist. For this point array exposure a beam current of 100 pA at 50 keV electron energy, corresponding to a beam diameter of about 15 nm, was used. Under appropriate development conditions [me-

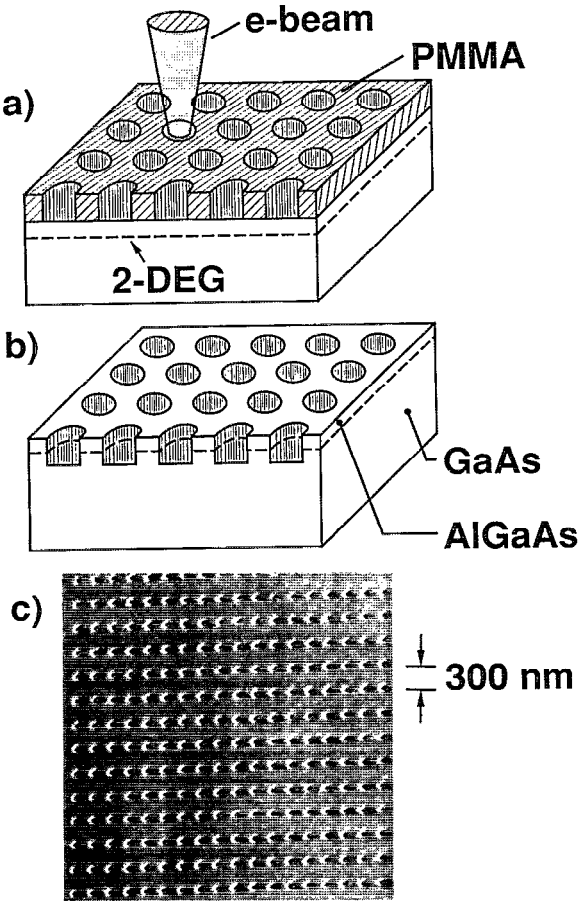

FIG. 1. (a) Schematic of pattern fabrication using electron beam lithography, and (b) etching an array of holes through the 2DEG. (c) An electron micrograph of the patterned surface (tilted by 45°).

[a]Present address: Bellcore, Red Bank, NJ.

 0003-6951/91/252960-03$02.00

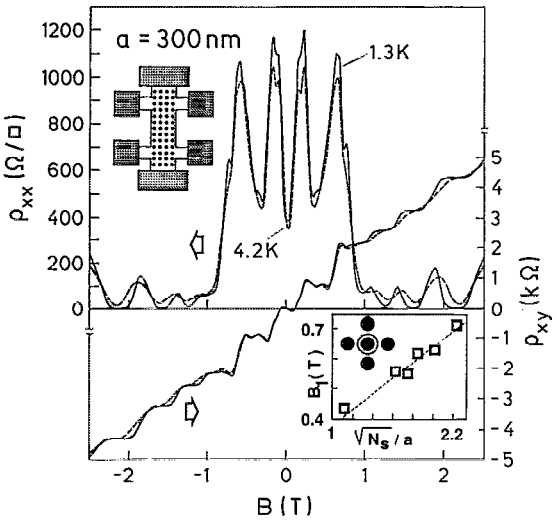

FIG. 2. Magnetoresistance and Hall resistance of the patterned device (top inset) measured for 1.3 and 4.2 K. The weak temperature dependence of the dominant low-field structure illustrates the semi-classical origin of the main features (see Ref. 15). The peak in ρ_{xx} around 0.6 T corresponds to a cyclotron orbit with diameter $2R_c = 2\sqrt{2\pi N_s}\hbar/eB_1 = a$ encircling one anti-dot (bottom inset). The linear dependence of B_1 on $\sqrt{N_s}/a$ (in units of 10^{14} m^2), measured on different samples, is shown in the inset (bottom).

thylisobutylketone (MIKB) and isopropylalcohol (IPA) 1:3], we are able to produce holes with diameters down to ~20 nm. For the samples described below the hole diameters d_{lith} range from 40 to 70 nm, whereas the periods were $a = 200$ nm and $a = 300$ nm.

In the next step the array of holes is transferred to the two-dimensional electron gas (2DEG) by deep mesa etching [sketched in Fig. 1(b)]. The etching process is the crucial point of the fabrication process since the 2DEG can be easily depleted from mobile electrons by inappropriate etching procedures. Using, e.g., ion milling (IBE) with 250 eV Ar ions one ends up with completely depleted devices for the same type of superlattice geometry and sample material. In our experiments the deep mesa etching is done by a reactive ion etching (RIE) process using $SiCl_4$ as the etchant. With optimized process parameters[12] it is possible to overcome problems of pure chemical (etches isotropically and limits therefore lateral resolution) or physical etching techniques. The degree of chemical etching is controlled via the $SiCl_4$ gas flow (50 sccm) and the process pressure (0.04 mbar), whereas the self-excited dc bias (100 V at power densities of 0.24 W/cm^2) minimizes the etching damage as described previously.[13] Using these parameters we etched *through* the 2DEG expecting a deep rectangular etching profile.[14] The etched depth was typically between 120 and 150 nm. The effective width of the etched holes, $d_{\text{eff}} = d_{\text{lith}} + 2l_{\text{depl}}$, which determines the sheet resistance consists of the lithographic hole diameter and the depletion length l_{depl} around those holes. An electron micrograph of the patterned section is shown in Fig. 1(c), demonstrating the homogeneity of the LSL. For electrical characterization this anti-dot superlattice is incorporated in a Hall bar geometry defined by conventional wet etching (sketched in the inset of Fig. 2). AuGeNi contacts alloyed at 450 °C contact the (now perforated) 2DEG. Our device geometry allows four-point measurements and therefore a proper determination of the sheet resistance $R_\square = \rho_{xx}(B = 0)$, magnetoresistance ρ_{xx}, and Hall resistance ρ_{xy}. Some of the samples have been polished to a total thickness of about 100 μm in order to use an evaporated Au layer as a backgate.

The effect of the imposed scatterers on magneto-resistance and Hall resistance is shown in Fig. 2. Compared to the unpatterned material ($R_\square = 20\Omega/\square$) the sheet resistance is significantly increased: the electron mean free path $l = \hbar k_F \mu/e$ ($\hbar$ = Planck's constant, k_F = Fermi wave vector, e = elementary charge), extracted from $R_\square = 370$ $\Omega/\square$ and the carrier density N_s (3×10^{11} cm^{-2}), is 510 nm, which is on the order of the superlattice period $a = 300$ nm. This indicates that the extrinsic anti-dot scattering mechanism dominates over the intrinsic processes such as impurity or acoustical phonon scattering. The magnetic field dependence of ρ_{xx} shows that the increase of the zero field resistance is not caused by an overall degradation of the material due to the processing. Increasing the magnetic field to a value where the cyclotron orbit diameter $2R_C$ becomes smaller than the period a results in a precipitous decrease of ρ_{xx}. At higher fields Shubnikov–de Haas oscillations emerge: above 1 T the magnetoresistance starts to oscillate around ~56 $\Omega/\square$. Within the Drude model this value corresponds to a mean free path $l = 3.3$ μm ($\mu = 370\,000$ cm^2/V s), comparable to the value measured in the unpatterned material ($l = 8$ μm, $\mu = 900\,000$ cm^2/V s). This indicates that the material between the etched holes essentially maintains the high quality of the unpatterned material.

The low-field ($2R_C > a - d_{\text{eff}}$) magnetotransport coefficients are dominated by the interplay between cyclotron radius R_c and the imposed period a (commensurability effect): for the sample shown in Fig. 2 peaks in ρ_{xx} and accompanying steps in ρ_{xy} appear at $2R_C = a$ and $2R_C = 3a$. The number of peaks and steps in this low-field regime depends on the cross section d_{eff}/a of the scatterers, and the magnetic field position of those features is connected to commensurate orbits, pinned upon small groups of anti-dots.[15] The total carrier density is reduced by the fraction of those pinned electrons and therefore both ρ_{xx} and ρ_{xy} are increased for commensurate magnetic fields. This pinning mechanism requires the absence of scattering centers on commensurate orbits (lifetime on orbit $\tau_{\text{orbit}} \gg \tau_{\text{ad}} \sim a/v_F$, the anti-dot scattering time) also confirming the high mobility of the electrons in between the anti-dots. In the inset of Fig. 2 the magnetic field B_1, corresponding to a pinned orbit around one anti-dot (see caption of Fig. 2), is plotted as a function of $\sqrt{N_s}/a$. The data points are taken from samples with different carrier density and different periodicity: their linear dependence demonstrates the commensurability between R_c and a.

The steep negative magnetoresistance around 0.75 T can be assigned to a reduction of backscattering in our periodic array which should be suppressed if the cyclotron diameter becomes smaller than $a - d_{\text{eff}}$.[16] We find that

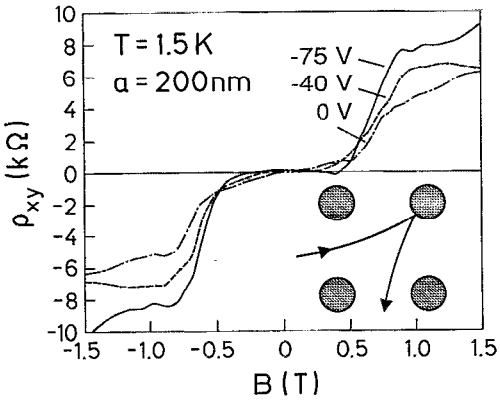

FIG. 3. Quenching of the Hall resistance for three carrier densities tuned by the backgate voltage V_g. The anti-dot superlattice consists of an array of *mesoscopic* Hall junctions (inset). The electron trajectory sketched in the inset causes a negative Hall slope (see Ref. 17).

transport now is essentially described by the intrinsic scattering rate of the unpatterned material. The magnetic field value corresponding to this transition might therefore be used to determine $l_{\text{depl}} = (d_{\text{eff}} - d_{\text{lith}})/2$.[6,8] For the data shown in Fig. 2 we estimate the depletion length l_{depl} to be $\sim$23 nm.

We have emphasized that the resistance within the low-field regime is determined by scattering from the anti-dots and that the transport between those etched holes is essentially ballistic. This seems to be the prerequisit for another phenomenon observed in such superlattices: the quenching of the Hall resistance around $B = 0$ (Figs. 2 and 3). This quench is even more pronounced in a sample with only 200 nm period (Fig. 3) where the Hall resistance is quenched over nearly 1 T. Such quenching has been observed in mesoscopic junctions[17] very similar to the region enclosed by four anti-dots in our device (Fig. 3, inset). Our samples, however, consist of typically 3×10^5 junctions and a theoretical explanation of this effect in superlattices is still missing. Our result might indicate that the quenching of the Hall effect in mesoscopic, single junctions is one special case and that in general a symmetrical arrangement of scatterers (boundaries in the single junction case) triggers the effect. This quenching of the Hall resistance has been observed recently also in an array of junctions defined by negatively biased gates.[18]

In summary, we have described the fabrication of an anti-dot-type superlattice with periods down to 200 nm. Maintaining an essentially defect-free electron gas between the etched holes, while the transport coefficients are determined by the periodic arrangement of scatterers, gives rise to variety of new superlattice effects.

We thank M. L. Roukes, A Scherer, and A. Forchel for valuable discussions, and M. Riek and E. Vasiliadou for their expert help in sample preparation.

[1] D. R. Hofstadter, Phys. Rev. B **14**, 2239 (1976).
[2] H. Sakaki, K. Wagatsuma, J. Hamasaki, and S. Saito, Thin Solid Films **36**, 497 (1976).
[3] H. Sakaki, Jpn. J. Appl. Phys. **28**, L314 (1989).
[4] U. Mackens, D. Heitmann, L. Prager, J. P. Kotthaus, and W. Beinvogel, Phys. Rev. Lett. **53**, 1485 (1984).
[5] G. Bernstein and D. K. Ferry, Superlatt. Microstruct. **2**, 373 (1986).
[6] M. L. Roukes and A. Scherer, Bull. Am. Phys. Soc. **34**, 633 (1989); A. Scherer and B. P. van der Gaag, Proc. SPIE **1248**, 149 (1990).
[7] K. Ismail, W. Chu, D. A. Antoniadis, and H. I. Smith, J. Vac. Sci. Technol. B **6**, 1824 (1988).
[8] K. Ensslin and P.M. Petroff, Phys. Rev. B **41**, 12307 (1990).
[9] H. Fang, R. Zeller, and P. J. Stiles, Appl. Phys. Lett. **55**, 1433 (1989).
[10] P. M. Petroff, A. C. Gossard, and W. Wiegmann, Appl. Phys. Lett. **45**, 620 (1984).
[11] W. Hansen, J. P. Kotthaus, and U. Merkt, in *Semiconductors and Semimetals* edited by M. Reed (Academic, in press).
[12] P. Grambow, T. Demel, D. Heitmann, M. Kohl, R. Schüle, and K. Ploog, Microcircuit Eng. **88**, 357 (1988).
[13] T. Demel, D. Heitmann, P. Grambow, and K. Ploog, Appl. Phys. Lett. **53**, 2176 (1988).
[14] P. Grambow, E. Vasiliadou, T. Demel, K. Kern, D. Heitmann, and K. Ploog, Microelectron. Eng. **11**, 47 (1990).
[15] D. Weiss, M. L. Roukes, A. Menschig, P. Grambow, K. von Klitzing, and G. Weimann, Phys. Rev. Lett. **66**, 27 May (1991).
[16] H. van Houten, C. W. J. Beenakker, P. H. M. van Loosdrecht, T. J. Thornton, H. Ahmed, M. Pepper, C. T. Foxon, and J. J. Harris, Phys. Rev. B **37**, 8534 (1988).
[17] M. L. Roukes, A. Scherer, and B. P. Van der Gaag, Phys. Rev. Lett. **64**, 1154 (1990), and references therein.
[18] C. G. Smith, M. Pepper, R. Newbury, H. Ahmed, D. G. Hasko, D. C. Peacock, J. E. F. Frost, D. A. Ritchie, G. A. C. Jones, and G. Hill, J. Phys. Condens. Matter **2**, 3405 (1990).